Article

Grafted Copolymer Electrolytes Based on the Poly(acrylic acid-*co*-oligo ethylene glycol acrylate) (P(AA-*co*-OEGA)) Ion-Conducting and Mechanically Robust Block

Achilleas Pipertzis, Martha Kafetzi, Despoina Giaouzi, Stergios Pispas,* and George A. Floudas*
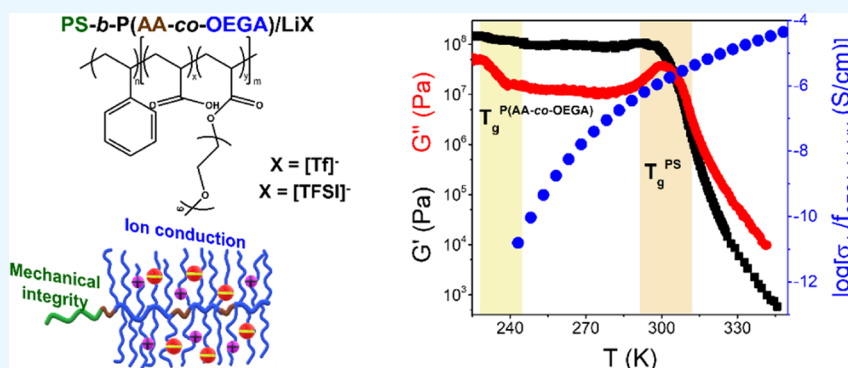
Read Online

ACCESS | Metrics & More | Article Recommendations | SI Supporting Information

ABSTRACT: A series of completely amorphous polymer brushes composed of grafted copolymer electrolytes based on the ion-containing block of poly(acrylic acid-*co*-oligo ethylene glycol acrylate) (P(AA-*co*-OEGA)) doped with $LiCF_3SO_3$ (LiTf) or $LiN(SO_2CF_3)$ (LiTFSI) and the glassy polystyrene (PS) block are synthesized and studied with respect to the structural, thermomechanical, and ion conduction properties. The incorporation of some AA units into the ion-conducting phase provides a trade-off between increased mechanical stability and anion/cation complexation. Consequently, the P(AA-*co*-OEGA) block can be engineered to simultaneously support ion conduction while exhibiting enhanced mechanical stability. Between the two anions ([Tf⁻] vs [TFSI⁻]), it is the latter that better supports the Li-ion transport. Diblock copolymer electrolytes doped with the larger anion ([TFSI⁻]) suppress ion complexation and give rise to superior ion conduction properties (by about 2 orders of magnitude), as compared to that of the smaller anion ([Tf⁻]). Overall, the PS-*b*-P(AA-*co*-OEGA)/LiTFSI diblock-random copolymer electrolyte with salt concentration, $r = 0.08$ (r is defined as the molar ratio of Li ions to EO units), best combines the required mechanical stability (storage modulus, $G' \sim 10^8$ Pa) with a relatively high dc-conductivity ($\sigma_{dc} \sim 10^{-6}$ S·cm⁻¹) at an ambient temperature (for application as solid polymer electrolytes (SPEs) in Li-ion batteries). This work suggests routes toward further improving the mechanical stability via the random incorporation of acids into the ion-containing block of nanophase-separated electrolytes.

KEYWORDS: *solid polymer electrolytes, ion conductivity, grafted copolymers, mechanical stability, poly(oligo ethylene glycol methacrylate) (POEGMA), polystyrene*

I. INTRODUCTION

Environmental pollution and the conventional oil-fuel crises are driving the demand for reliable rechargeable Li-ion batteries with fast charge/discharge rates and high energy densities.[1−5] The latter is necessary for storing the excess energy produced from renewable energy sources, e.g., the solar energy. In addition, Li-batteries give power to portable electronic devices, electrified transportation, autonomous homes and businesses, as well as machines of current technological interest, such as drones and robots. However, conventional liquid electrolytes are flammable and toxic, involving a risk of serious safety (e.g., battery explosion, leakage, etc.) and performance (e.g., short-circuit, etc.) problems.[3,4] To alleviate these serious safety issues and, at the same time, to increase the energy density and lifetime

of a battery, improvement of the mechanical integrity (storage modulus, $G' \sim 0.1$ GPa) through the design of solid polymer electrolytes (SPEs) is sought. However, the ionic conductivities of SPEs are lower ($\sigma_{dc} < 10^{-3}$ S·cm⁻¹) as compared to liquid ones, suggesting that further improvements are necessary to meet the demands of future battery technologies.

Over the past decades, the scientific interest has turned to nanophase-separated block copolymer electrolytes that combine the "liquid-like" conductive phase of poly(ethylene oxide) (PEO) doped with Li salt (reflecting mainly its capability for Li salt dissociation and its low glass temperature T_g)[6−12] with a "high-T_g nanophase", usually polystyrene (PS).[13−21] In block copolymers, the segregation strength is determined by the product, χN, where χ is the Flory−Huggins interaction parameter, associated with the thermodynamic compatibility between A and B blocks and N is the total degree of polymerization.[22] However, the main factor that impedes ion transport in copolymers based on linear chains of PEO is the strong tendency for crystallization, as well as the formation of crystalline complexes with certain Li salts. Attempts have been made to suppress the crystallinity mainly by modifying the polymer architecture (e.g., grafted architecture,[23−29] tapered copolymers[30−33]). Parenthetically, tapered copolymers combine nanostructured morphologies (double gyroid,[32] cylindrical or perforated layers[33]) favorable for Li-ion transport, with improved segmental mobility and excellent mechanical properties (toughness and strain at break exceeding 900%) as compared to their normal copolymers.[30−33] Moreover, the tendency for crystalline complex formation can be tuned by changing the lithium salt. The usual salts for this purpose are lithium bis (trifluoromethanesulfonyl)imide (LiTFSI) and lithium triflate (LiTf), with the former being superior, as it suppresses complex formation.[9,14,16,21]

Electrolytes composed of short PEO chains densely grafted on a PS backbone were proposed earlier by us.[23] The densely *grafted* architecture with short PEO chains enhances the segmental mobility and suppresses/reduces the tendency for PEO crystallization and complex crystal formation, resulting in a combination of relatively high elastic modulus ($G' \sim 2 \times 10^6$ Pa) with comparably high ionic conductivity ($\sigma' \sim 6 \times 10^{-5}$ S·cm^{-1}).[23] Furthermore, a significant decrease of PEO crystallinity on going from linear to comb-like architecture was reported for PS-*b*-PEO diblock copolymers.[24] Hence, the *grafted* architecture with a comb-like chain topology is advantageous over linear ones for designing fully amorphous SPEs.[23−29]

A promising comb-like (branched-like) homopolymer electrolyte that combines the *grafted* architecture and the beneficial characteristics of PEO is the poly(oligo ethylene glycol methacrylate) (POEGMA).[26−28] POEGMA and its acrylic analogue poly(oligo ethylene glycol acrylate) (POEGA) have the advantage of being biocompatible. As such, they have been employed in drug delivery applications.[34−37] Specifically, POEGMA (POEGA) consists of a methyl meth(acrylate) backbone and ethylene glycol side groups. Despite its rigid backbone, the segmental dynamics and the associated T_g are dominated by the EO side chains and are similar to that of PEO.[27] At the same time, it exhibits high dielectric permittivity ($\varepsilon'_{POEGMA} \sim 10$), which is typically twice that of PEO, suggesting an increasing tendency for anion−cation dissociation.[27] Evidently, the combination of the densely grafted backbone with the *short* ethylene glycol side groups is anticipated to suppress crystallinity and enhance segmental mobility, thus engineering high ionic conductivities. These favorable characteristics of POEGMA motivated studies of SPEs.[30,32,38−47]

Herein, we build on these ideas and further design and synthesize a series of grafted block-random diblock (PS-*b*-P(AA-*co*-OEGA)) and triblock (PS-*b*-P(AA-*co*-OEGA)-*b*-PS) copolymer electrolytes composed of a high-T_g block (PS) that provides the mechanical stability and a densely grafted ion-containing block comprised of randomly distributed acrylic acid (AA) and OEGA repeat units. AA was incorporated in the ion-conducting phase as a means to trigger the interaction parameter and to increase the incompatibility between the ionic and the nonionic blocks (the reported $\chi_{PS-PAA} \sim 0.883$[48] is drastically higher than $\chi_{PS-POEGMA} \sim 0.1$ at 303 K).[31,38,40] Moreover, AA stiffens the backbone of the P(AA-*co*-OEGA) block due to its high T_g, thus improving the mechanical stability. At the same time, its small content and random distribution along the backbone preserve the enhanced segmental mobility of the short EO side groups. In this study, four different salt concentrations, with r (=[Li$^+$]/[EO]) = 0.06, 0.08, 0.13, and 0.25, were studied and two different anions ([Tf$^-$] and [TFSI$^-$]) were employed. Between the two anions, the larger and weakly coordinated [TFSI$^-$] is the preferred one for Li-ion transport. PS-*b*-P(AA-*co*-OEGA)/LiTFSI copolymers combine the required mechanical stability ($G' \sim 10^8$ Pa) with conductivity values up to $\sim 10^{-6}$ S·cm^{-1} at an ambient temperature or up to 2×10^{-5} S·cm^{-1} at $T = 333$ K, e.g., at operational temperatures for Li-ion batteries.

II. EXPERIMENTAL SECTION

II.I. Synthesis of PS-*b*-P(AA-*co*-OEGA). The PS-*b*-P(AA-*co*-OEGA) block-random diblock terpolymer was prepared by utilizing the RAFT polymerization methodology. First, a PS homopolymer was synthesized. Subsequently, PS acted as the macro-RAFT agent for the copolymerization of acrylic acid (AA) and (oligo ethylene glycol) methyl ether acrylate (OEGA) to form the P(AA-*co*-OEGA) random second block and to finally receive the PS-*b*-P(AA-*co*-OEGA) block-random terpolymer.

In a 25 mL round-bottom flask, equipped with a magnetic stirrer, 1.5 g (0.0144 mol) of styrene, which was previously purified by passing through a packed column filled with inhibitor removers (to remove inhibitor traces), 0.137 g (0.375 mmol) of 2-(dodecylthiocarbono-thioylthio)-2-methylpropionic acid, AIBN (0.0062 g, 0.0375 mmol), and 3 mL of 1,4-dioxane were inserted. The flask was sealed with a rubber septum. The reaction solution was degassed by a high-purity nitrogen gas bubbling for 20 min and was placed in an oil bath at 353 K for 12 h. Afterward, the polymerization was terminated by cooling the mixture at 253 K and exposing it to air. The PS homopolymer was precipitated in excess of MeOH to exclude the unreacted monomer. The product was collected after drying in a vacuum oven at 278 K for 48 h (yield 48%). Subsequently, PS was used as the macro-RAFT agent to synthesize the P(AA-*co*-OEGA) random second block.

To prepare the PS-*b*-P(AA-*co*-OEGA) block-random terpolymer, PS macro-RAFT (0.2 g, 0.107 mmol), acrylic acid (AA) (0.45 g, 6.244 mmol), (oligo ethylene glycol) methyl ether acrylate (0.45 g, 0.938 mmol), AIBN (0.0065 g, 0.04 mmol), and 6.4 mL of 1,4-dioxane were added in a 25 mL round-bottom flask. AA and OEGA monomers were also purified by passing through an inhibitor-removing resin. The reaction mixture was degassed by a high-purity nitrogen gas bubbling for 20 min and then submerged in an oil bath at 343 K for 24 h. The polymerization was quenched by adjusting the temperature of the mixture to 253 K and exposure to air. Subsequently, the diblock terpolymer was precipitated in excess *n*-hexane for removal of the unreacted monomers and then left for 48 h inside a vacuum oven at 298 K to dry (yield 65%).

II.II. Synthesis of PS-*b*-P(AA-*co*-OEGA)-*b*-PS. The PS-*b*-P(AA-*co*-OEGA)-*b*-PS triblock terpolymer was synthesized using RAFT polymerization strategy. To obtain PS-*b*-P(AA-*co*-OEGA)-*b*-PS, at first PS bifunctional macro-RAFT agent was prepared by selecting the S,S-dibenzyl trithiocarbonate as the fitting CTA agent. Following this, the P(AA-*co*-OEGA) random block was incorporated to finally acquire PS-*b*-P(AA-*co*-OEGA)-*b*-PS. One gram (0.0096 mol) of styrene, which was previously purified by passing through a packed column filled with inhibitor removers, 0.109 g (0.375 mmol) of S,S-dibenzyl trithiocarbonate, AIBN (0.00123 g, 0.075mmol), and 6 mL of 1,4-dioxane were

introduced in a single-neck round-bottom flask along with a magnetic stirrer. The flask was fitted with a rubber septum. The final mixture was degassed by a high-purity nitrogen gas bubbling for 20 min and was inserted in an oil bath at 353 K for 12 h. Afterward, the polymerization was terminated by cooling the mixture at 253 K and exposing it to air. The PS homopolymer was precipitated in excess of cold MeOH to exclude the unreacted monomer. The product was collected after drying in a vacuum oven at 298 K for 48 h (yield 54%).

Subsequently, 0.4 g (0.833 mmol) of OEGA, 0.7 g (9.714 mmol) of AA, 0.25 g (0.1 mmol) of PS difunctional macro-RAFT agent, 3.33 mg (0.02 mmol) of AIBN, and 9.2 ml of 1,4-dioxane were placed in a round-bottom flask. Monomers were also purified by carrying out the previously stated procedure. The same degassing process was implemented, and afterward, the flask was introduced in an oil bath at 343 K for 24 h. The polymerization was terminated by cooling the mixture at 253 K and exposing it to air. The resulting triblock terpolymer was precipitated in excess of n-hexane to draw out unreacted monomers. The final product was obtained after drying in a vacuum oven at 298 K for 48 h (yield 75%).

^{1}H-NMR and SEC characterization data for the diblock and triblock copolymers are provided in Figures S1–S4, Supporting Information section.

II.III. Synthesis of POEGMA Homopolymer. For comparison purposes, a POEGMA homopolymer of 33.0×10^3 g·mol^{-1} was also synthesized. The synthetic process is described as follows: 3 g (6.32 mmol) of (oligo ethylene glycol) methyl ether methacrylate (OEGMA), 25.4 mg (0.091 mmol) of 4-cyano-4-(phenyl-carbonothioylthio)pentanoic acid, 2.98 mg of AIBN (0 g, 0.018 mmol), and 12 mL of 1,4-dioxane were added in a 25 mL round-bottom flask where a magnetic stirrer was previously added. OEGMA was purified before use by passing through inhibitor-removing resins. Degassing of the mixture was made using a high-purity nitrogen gas bubbling for 20 min, and eventually the flask was sunk in an oil bath at 343 K for 24 h. The polymerization was quenched by adjusting the temperature of the mixture to 253 and exposure to air. Subsequently, the POEGMA homopolymer was precipitated in excess n-hexane for removal of the unreacted monomer and then left for 48 h inside a vacuum oven at 298 K to dry (yield 78%).

Copolymer electrolytes were doped with LiTf or LiTFSI at four Li salt concentrations: $r = [Li^+]/[EO] = 0.06, 0.08, 0.13,$ and 0.25. The chemical structure of the investigated block-random electrolytes is depicted in Figure 1. Moreover, the respective POEGMA homopolymer electrolytes, bearing the same Li salts, were also prepared.

II.IV. Differential Scanning Calorimetry. The thermal properties of the POEGMA homopolymer and the PS-b-P(AA-co-OEGA) diblock and PS-b-P(AA-co-OEGA)-b-PS triblock copolymer electrolytes were studied by differential scanning calorimetry (DSC) with a Q2000 (TA Instruments). The instrument was calibrated for best performance in

the specific temperature range and heating/cooling rate. The calibration sequence included a baseline calibration for the determination of the time constants and capacitances of the sample and reference sensor using a sapphire standard. In the next step, an indium standard (ΔH = 28.71 J/g, T_m = 428.8 K, with a heating rate of 10 K·min^{-1}) was employed for the enthalpy and transition temperature calibration. Following the indium calibration, a baseline measurement verified the successful calibration of the instrument. Concerning the heat capacity calibration, a temperature-modulated DSC (TM-DSC) calibration was made with a sapphire standard. Samples (typically ~5–6 mg) were hermetically closed in an aluminum pan and placed on a sample sensor. An empty aluminum pan was used as a reference. The temperature protocol involved the first cycle of cooling and heating with a rate of 10 K·min^{-1} to erase the sample's thermal history, followed by a second cycle with the same rate in the temperature range from 173 to 423 K.

II.V. Small-Angle X-ray Scattering (SAXS). SAXS measurements were made using Cu Kα radiation (RigakuMicroMax 007 X-ray generator, Osmic Confocal Max-Flux curved multilayer optics). Oriented fibers of 1.0 mm diameter were prepared by a mini-extruder. 2D scattering patterns were recorded on a Mar345 image plate at a sample-to-detector distance of 2.11 m. The recorded intensity distributions were integrated along the equatorial and meridional axes of the 2D images and are discussed as a function of the modulus of the scattering vector, q ($q = (4\pi/\lambda) \sin(2\theta/2)$, where λ is the wavelength λ = 0.154184 nm and 2θ is the scattering angle). Temperature-dependent SAXS measurements for the diblock and triblock copolymer electrolytes with Li salt concentration, r = 0.08 ([EO]/[Li$^+$] = 12:1), were carried out in the temperature range from 303 to 423 K on heating and subsequent cooling, in steps of 30 K. Measurements were of 1 h long following another hour of equilibration at each temperature.

II.VI. Dielectric Spectroscopy. Dielectric spectroscopy (DS) measurements were performed with a Novocontrol α frequency analyzer. The temperature protocol involved measurements within the range from 223 to 383 K in steps of 5 K and for frequencies in the range from 10^{-2} to 10^7 Hz under isobaric conditions. The dielectric cell consisted of two electrodes, 20 mm in diameter, and the sample with a thickness of 100 μm, maintained by Teflon spacers. Samples were prepared as melts under vacuum by pressing the electrodes to the spacer thickness. The complex conductivity function, $\sigma^* = \sigma' + i\sigma''$, where σ' and σ'' are the real (i.e., the dc-conductivity) and imaginary parts, respectively, has been obtained as a function of angular frequency, ω, and temperature, T.[49,50] To extract the dc-conductivity, the plateau in the real part σ' was used. An alternative way to obtain the dc-conductivity is from the random free-energy barrier model (RBM).[51,52]

II.VII. Rheology. A TA Instrument AR-G2 with a magnetic bearing that allows for nanotorque control was used for recording the viscoelastic properties of the polymer electrolytes. Measurements were made with the environmental test chamber (ETC) as a function of temperature. The samples were prepared on the lower rheometer plate (8 mm). Then, the upper plate was brought into contact and the thickness was adjusted. Temperature control was achieved within 0.1 K with a nitrogen convection oven. The linear and nonlinear viscoelastic regions were identified through the strain amplitude dependence of the complex shear modulus, $|G^*(\omega)|$, at ω = 10 rad·s^{-1}. Two types of measurements were carried out: (i) isochronal temperature ramps with ω = 10 rad·s^{-1} between 213 and 383 K and (ii) isothermal frequency sweeps within the range $10^{-1} < \omega < 10^2$ rad·s^{-1} at some selected temperatures.

III. RESULTS AND DISCUSSION

III.I. Ion Conduction in Comb-Like POEGMA/LiX Homopolymer Electrolytes. Quantitative insight into the factors (e.g., thermodynamics, anion type, etc.) that dictate the ion conduction mechanism of comb-like homopolymer electrolytes can be obtained by a combination of thermodynamic (DSC) and dynamic (DS) measurements. A side group length comprising nine EO units was employed because it was found to
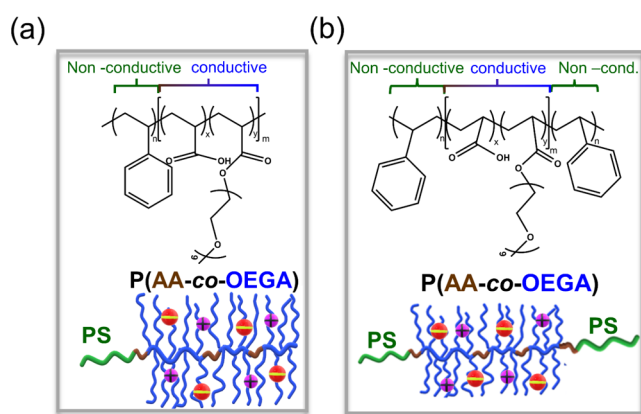

Figure 1. Chemical structure of the investigated SPEs based on (a) PS-b-P(AA-co-OEGA) diblock copolymer and (b) PS-b-P(AA-co-OEGA)-b-PS triblock copolymer.
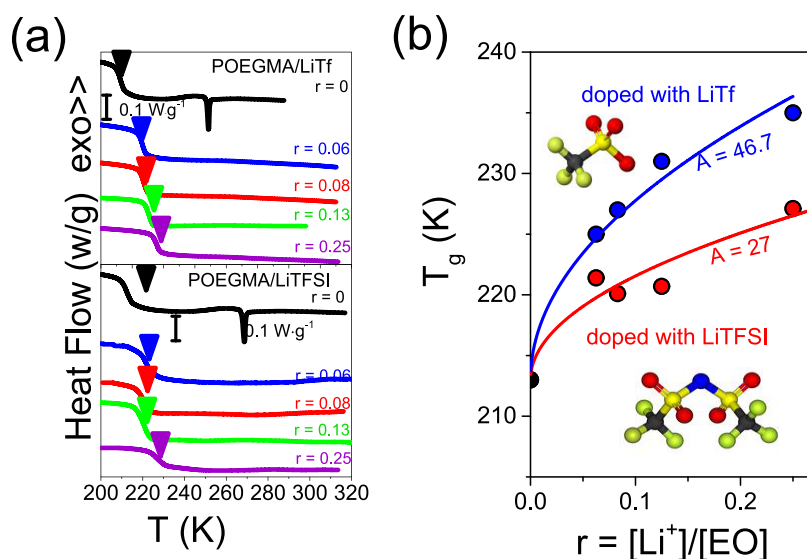
Figure 2. (a) DSC thermograms for POEGMA homopolymer electrolytes doped with (top) LiTf and (bottom) LiTFSI at four salt concentrations with $r = 0.06$ (blue line), $r = 0.08$ (red line), $r = 0.13$ (green line), and $r = 0.25$ (purple line) during the second heating run with a rate of 10 K·min^{-1}. Vertical arrows give the respective T_g's. (b) Calorimetric T_g as a function of Li salt concentration, $r = ([Li^+]/[EO])$ for POEGMA doped with LiTf (blue) and LiTFSI (red). The solid lines are fits to eq 1.
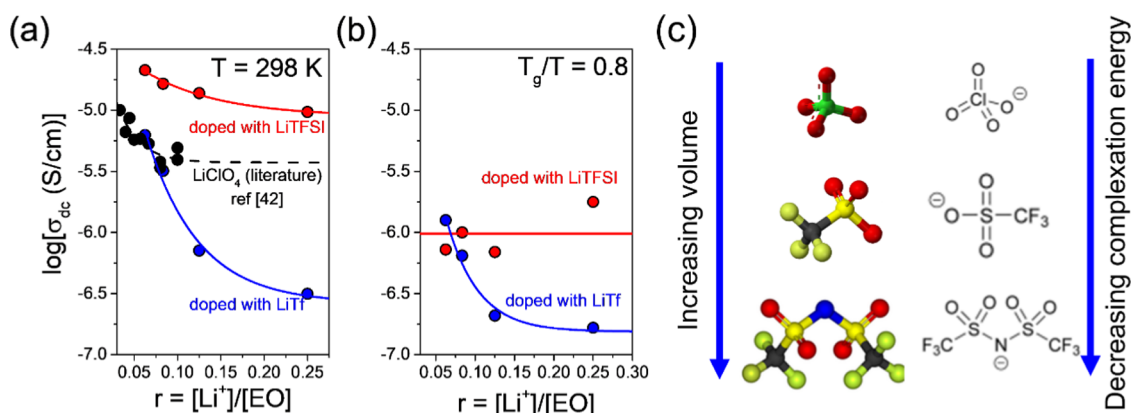

Figure 3. Ionic conductivity as a function of salt concentration for the POEGMA homopolymer electrolytes doped with LiTf (blue symbols) and LiTFSI (red symbols) at (a) an ambient temperature and (b) at a T_g-scaled temperature of $T_g/T = 0.8$. Literature data for POEGMA/LiClO$_4$ (black symbols) electrolytes are also included.[42] (c) van der Waals volumes of the different anions.

be the preferred EO length for Li-ion transport in salt-doped POEGMA electrolytes.[42] The thermodynamic characteristics of the POEGMA homopolymer electrolytes doped with LiTf or LiTFSI are discussed with respect to Figure 2.

The heat flow of the neutral POEGMA homopolymer exhibits a step-like decrease at T_g (~213 K) followed by an endothermic peak at higher temperatures, signifying the melting of POEGMA crystals. Following doping with LiTf or LiTFSI, the crystallization/melting peak is suppressed, leading to completely amorphous electrolytes, a highly desirable feature for SPEs. The disruption of the crystalline structure is attributed to ion associations with the POEGMA. Specifically for $r = 0.08$, the POEGMA/LiTFSI (LiTf) exhibits a T_g at about 220 (227) K, which is ~10 K (~4 K) lower than that of PEO/LiTFSI (LiTf) electrolytes.[9,12] As depicted in Figure 1b, T_g increases by about 10 K (6 K), with increasing Li salt content for the homopolymer electrolytes doped with LiTf (LiTFSI). Specifically, T_g increases as

$$T_g(K) = T_g^0 + A(r)^{1/2} \qquad (1)$$

where T_g^0 is the calorimetric glass temperature of neutral POEGMA and A is a dimensionless parameter. Moreover, the homopolymer electrolytes doped with LiTFSI exhibit lower T_g values, as compared to LiTf. Because of its smaller size, LiTf interacts more strongly with the EO units in the side groups of POEGMA. The stronger binding makes the backbone dynamics more sluggish, increasing the T_g. On the other hand, the lower T_g of electrolytes doped with LiTFSI is anticipated to enhance the Li-ion conductivity.

Ion conduction in the POEGMA electrolytes doped with LiTf or LiTFSI is discussed next. The dc-conductivity was extracted from the frequency-independent region of $\sigma'(\omega)$ curves (plateau) (Figure S5). The higher (lower)-frequency region is associated with the ac-conductivity (electrode polarization). The $\sigma_{dc}(T)$ for the homopolymer electrolytes, as well as of the neutral POEGMA, is further discussed with respect to Figure S5. The $\sigma_{dc}(T)$ for the neutral POEGMA homopolymer reflects the structural changes (melting) (Figures 2 and S6). On the other hand, the $\sigma_{dc}(T)$ of the fully amorphous POEGMA electrolytes doped with LiTf or LiTFSI conforms to the Vogel−Fulcher−

Table 1. Average Molar Mass, Dispersity, Đ, Molar Mass of PS Determined by Size-Exclusion Chromatography (SEC), as well as the Weight Fractions of Different Blocks (PS, PAA, and POEGA) Extracted from ^{1}H-NMR Measurements

sample[a]	M_w (g·mol^{-1})[b,c]	Đ PS[c]	M_w^{PS} (g·mol^{-1})	% PS[b]	% PAA[b]	% POEGA[b]
PS-*b*-P(AA-*co*-OEGA)	16,500	1.06	2800	17	5	78
PS-*b*-P(AA-*co*-OEGA)-*b*-PS	7800	1.31	2500	32	8	60

[a]Abbreviations for the sample structures are explained in the experimental part. [b]Determined via ^{1}H-NMR. [c]Determined via SEC.
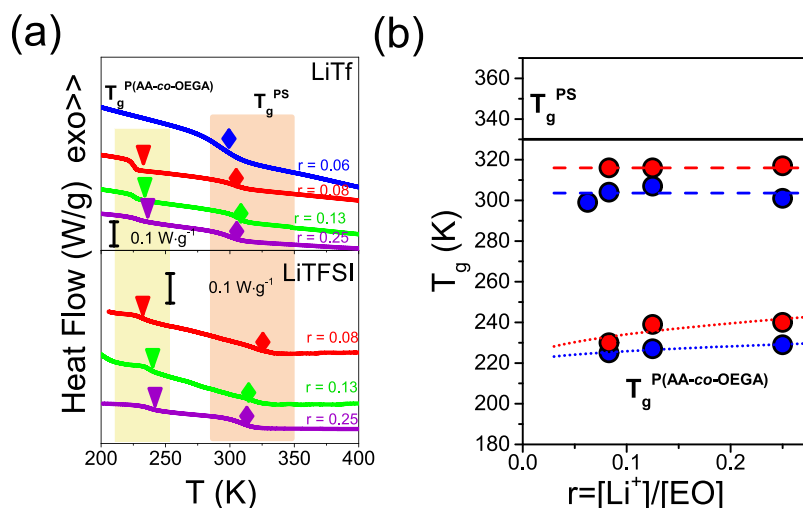

Figure 4. (a) DSC thermograms for PS-*b*-P(AA-*co*-OEGA) block-random copolymer electrolytes doped with (top) LiTf and (bottom) LiTFSI at four salt concentrations with $r = 0.06$ (blue line), $r = 0.08$ (red line), $r = 0.13$ (green line), and $r = 0.25$ (purple line) upon the second heating run with a rate of 10 K·min^{-1}. The arrows and rhombi indicate the $T_g^{P(AA-co-OEGA)}$ and T_g^{PS}, respectively. (b) Calorimetric T_g as a function of Li salt concentration, $r = ([Li^+]/[EO])$ for PS-*b*-P(AA-*co*-OEGA) doped with LiTf (blue symbols) and LiTFSI (red symbols). The respective dashed (dotted) lines represent linear fits (fits to eq 1). The solid black line indicates the T_g^{PS}.[58]

Tammann (VFT) equation written for the conductivity contribution as

$$\sigma_{dc}(T) = \sigma_0^\# \exp\left(-\frac{B}{T - T_0}\right) \tag{2}$$

where $\sigma_0^\#$ is the dc-conductivity in the limit of very high temperatures, B is the activation parameter, and T_0 is the "ideal" glass temperature, which differs from the calorimetric T_g by ~40–50 K. The VFT parameters of the POEGMA electrolytes are provided in Table S1.

The ionic conductivity as a function of salt concentration for the POEGMA electrolytes can be discussed with the help of Figure 3. At an ambient temperature, the POEGMA/LiTFSI exhibits higher dc-conductivity as compared to LiClO$_4$- or LiTf-doped electrolytes, reflecting the weaker association and the lower T_g of the LiTFSI-doped electrolytes. In addition, dc-conductivity decreases with increasing salt concentration following the increase in T_g (Figure 2b). Evidently, a major factor that dictates ion transport in POEGMA homopolymer electrolytes is the T_g. However, when compared at a fixed normalized temperature relative to T_g (i.e., at a fixed T_g/T), the ionic conductivity of POEGMA/LiTf is lower than in POEGMA/LiTFSI for the electrolytes with the higher ion content. The higher ionic conductivity of POEGMA/LiTFSI reflects the absence of ion complexation.[29,53−55] According to the results from recent DFT calculations,[53] among the different anions investigated, [TFSI]$^-$ exhibited one of the lowest complexation energies. This is a composite effect, reflecting the large anion size, the charge delocalization along the S−N−S bonds, and steric effects. Hence, [TFSI$^-$] is preferable for Li-ion conduction. At an ambient temperature, the maximum dc-

conductivity of the POEGMA/LiTFSI electrolytes is ~2 × 10^{-5} S·cm^{-1} for $r = 0.06$. However, POEGMA/LiTFSI electrolytes are liquids at an ambient temperature (Figure S7), suggesting that a combination with high T_g and mechanically robust block(s) is the necessary next step.

III.II. PS-*b*-P(AA-*co*-OEGA) Copolymer Electrolytes. The ion-containing phase of the copolymer electrolytes is now modified so as to provide high ionic conductivity (through the mobile EO/Li side groups) and improved mechanical stability (through the modified backbone). Specifically, it is now composed of randomly distributed AA units along the OEGA backbone. Instead of OEGMA repeat units, its acrylic analogue, OEGA, was used here for designing copolymers with well-defined molecular characteristics (all components belong to the "family" of acrylates) (Table 1). The glass temperature of POEGA ($T_g^{POEGA} \sim 209$ K)[56] is slightly lower than that of POEGMA ($T_g^{POEGMA} \sim 213$ K; Figure 2) while keeping the same EO side group length. It is well documented in the literature[27,57] that the dominant factor that governs the segmental dynamics and the associated T_g in comb-like polymers is the (EO) side group length due to the internal plasticization effect (e.g., faster backbone dynamics by the incorporation of short and very mobile side groups). The thermodynamics of the PS-*b*-P(AA-*co*-OEGA) copolymer electrolytes doped with LiTf or LiTFSI, as well as the impact of the AA incorporation on the T_g of the conductive phase, can be discussed with respect to Figure 4.

The DSC traces of the PS-*b*-P(AA-*co*-OEGA) block-random copolymer electrolytes doped with LiTf or LiTFSI display two T_gs: a lower T_g at ~ 225 K and a higher T_g within the temperature range of ~300−320 K for Li salt concentrations
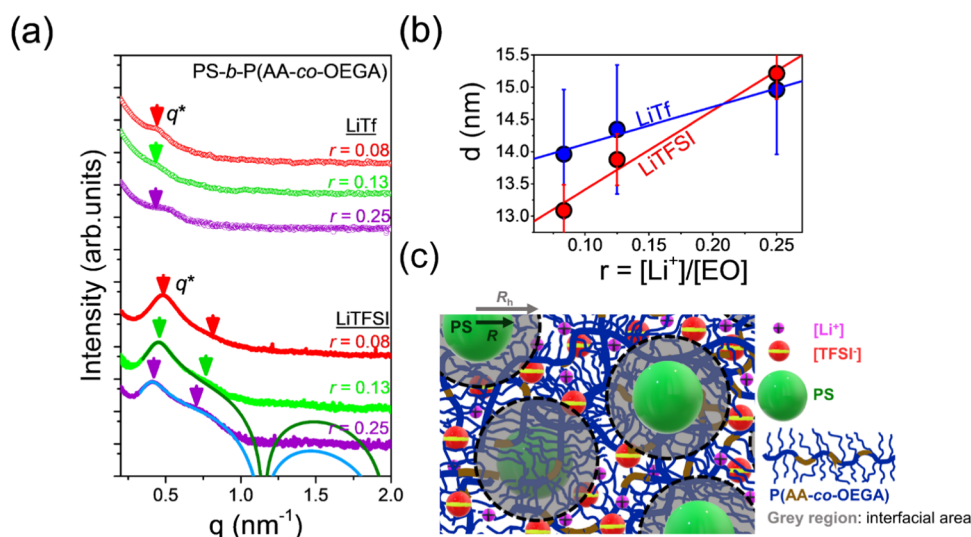
Figure 5. (a) SAXS patterns for the PS-*b*-P(AA-*co*-OEGA) copolymer electrolytes doped with LiTf (symbols) and LiTFSI (lines) at three salt concentrations: $r = 0.08$ (red), $r = 0.13$ (green), and $r = 0.25$ (purple), at $T = 303$ K. The vertical arrows give the positions of interference peaks from disordered spheres. The olive (blue) line represents the Percus–Yevick hard-sphere model (eq 3) of the SAXS pattern for the electrolyte doped with LiTFSI at $r = 0.13$ ($r = 0.25$). (b) Domain spacing as a function of salt concentration, r, for diblock copolymer electrolytes doped with LiTf (blue symbols) and LiTFSI (red symbols). (c) Schematic representation of the copolymer morphology.

with $r \geq 0.08$. The lower (higher) T_g is associated with the vitrification of the AA-*co*-OEGA (PS) segments, implying some local segregation between the two blocks. The random incorporation of AA along the POEGA backbone increases the $T_g^{\text{P(AA-}co\text{-OEGA)}}$ by about ∼5 K, as compared to the respective $T_g^{\text{POEGMA/LiX}}$ (Figure 2). Moreover, the $T_g^{\text{P(AA-}co\text{-OEGA)}}$ slightly increases (by about 4−10 K) with increasing Li salt concentration, reflecting the anion/cation complexation with the carbonyl group in PAA.[59,60] Future efforts would emphasize on the effect of PAA content on the glass temperature (and dc-conductivity) of the P(AA-*co*-OEGA) phase. Precise information about the degree of segregation between the salt-containing (P(AA-*co*-OEGA)) and "mechanical" block (PS) can be obtained by X-ray measurements. On the other hand, XRD measurements further show that the PS-*b*-P(AA-*co*-OEGA) block-random copolymer electrolytes doped with LiTf and LiTFSI are amorphous (Figure S8).

III.III. Copolymer Morphology. The SAXS patterns of the PS-*b*-P(AA-*co*-OEGA) diblock copolymer electrolytes are given in Figure 5.

As shown in Figure 5a, the PS-*b*-P(AA-*co*-OEGA)/LiTf electrolytes, for $r = 0.08$, exhibit only a broad peak, at $q^* \sim 0.45$ nm^{-1}, suggesting mixing between the two blocks. On the other hand, the SAXS patterns of the same electrolytes doped with LiTFSI exhibit some additional features. Apart from the stronger peak at q^*, it develops some additional broad features at higher q. These features suggest the formation of weakly ordered PS spheres (83% of the P(AA-*co*-OEGA) ion-conducting phase).

In this case, the scattered intensity is given by the product[61]

$$I(q) \sim K \cdot P(q) \cdot S(q) \tag{3}$$

where $P(q)$ is the form factor and $S(q)$ is the structure factor. The structure factor of the low-q interference peak (indicated with vertical arrows in Figure 5a) associated with the inter-sphere correlations can be described by the Percus–Yevick model applicable to a fluid of hard spheres, as[61]

$$S(q, f_h, R_h) = \cfrac{1}{1 + \cfrac{24 f_h\, G(A)}{A}} \tag{4}$$

where $A = 2qR_h$ and R_h and f_h are the effective radius and the effective volume fraction of PS spheres, respectively, and $G(A) = \frac{\alpha}{A^2}(\sin A - A\cos A) + \frac{\beta}{A^3}(2A\sin A + (2 - A^2)\cos A - 2) + \frac{\gamma}{A^5}(-A^4\cos A + 4[(3A^2 - 6)\cos A + (A^3 - 6A)\sin A + 6])$.[61] The form factor of homogeneous spheres with a radius R is given by[61]

$$P(q) = u_0{}^2 \left[\frac{3}{(qR)^3}[\sin(qR) - qR\cos(qR)] \right]^2 \tag{5}$$

where u_0 is the sphere volume. The simulation of the experimental scattering curve with the above theoretical model (eq 3) requires a set of five ($R \sim 3.9$ (4.5) nm, $R_h \sim 5.4$ (5.3) nm, $\alpha \sim -0.6$ (4.2), $\beta \sim 3.7$ (2.2), and $\gamma \sim -13.2$ (−2.5) for $r = 0.13$ (0.25)) fitting parameters. The effective volume fraction can be calculated from the effective radius as $f_h \sim f_0 \times (R_h/R)^3$, where f_0 (∼0.18) is the initial volume fraction of PS spheres. The radius of PS spheres ($R \sim 3.9$ nm) can also be extracted from the position of the first minima in the form factor (at $qR = 4.484$) based on eq 5.[61,62] This estimate matches quantitatively the root-mean-square end-to-end distance of the PS chains that amounts to $\langle r^2 \rangle^{1/2} \sim (Nb^2)^{1/2} \sim 3.5$ nm, where N ($= M/M_0$, $M_0 = 720$ g·mol^{-1}) is the number of Kuhn monomers and b (= 1.8 nm) is the Kuhn length.[63] The larger effective sphere radius and volume fraction reflect the presence of mixed PS/P(AA-*co*-OEGA) domains at the interface with an estimated thickness of $R_h - R = 1.5$ (0.8) nm for $r = 0.13$ (0.25) nm. Notice that the interfacial thickness decreases with increasing salt concentration, as anticipated from PEO-based electrolytes.[13] A schematic representation of the PS spherical morphology in the disordered state, which includes the interfacial area (gray region), is provided in Figure 5c.

By increasing Li salt concentration, the domain spacing increases linearly as $d = 12.2 + 12.3r$ ($d = 13.5 + 5.7r$) for the random diblock copolymer electrolytes doped with LiTFSI (LiTf) (Figure 5b).[13−20,31,38,40] The increase in domain spacing
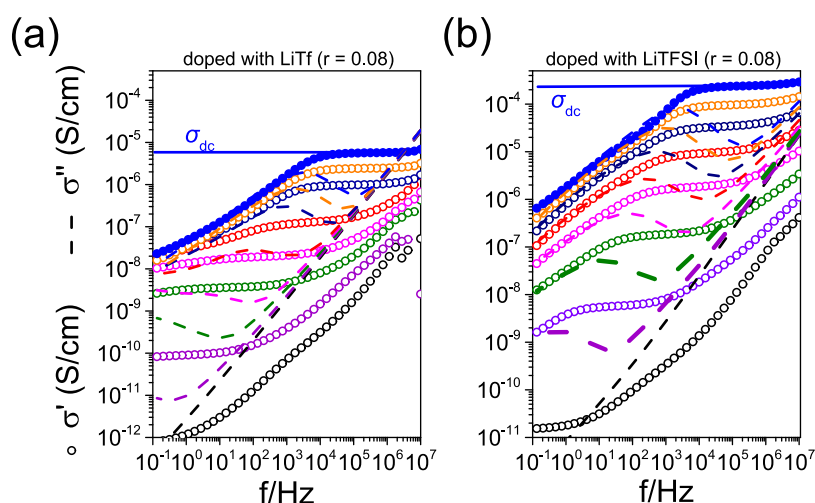
Figure 6. Real (symbols) and imaginary (dashed lines) parts of the complex conductivity function, $\sigma^*(\omega)$, for PS-*b*-P(AA-*co*-OEGA) block-random copolymer electrolytes doped with (a) LiTf and (b) LiTFSI at a fixed Li salt concentration, $r = 0.08$ ([EO]/[Li$^+$] = 12:1), shown at some selected temperatures: 243 K (black symbols), 263 K (purple symbols), 283 K (olive symbols), 303 K (magenta symbols), 323 K (red symbols), 343 K (navy symbols), 363 K (orange symbols), and 383 K (blue symbols).

reflects the increase in the effective Flory−Huggins interaction parameter, χ_{eff}. The latter can be accurately obtained from the structure factor by fitting to the random phase approximation theory in the disordered state. However, the order-to-disorder transition temperature for the PS-*b*-P(AA-*co*-OEGA)/LiTFSI electrolytes was not accessible (Figure S9). In polymer electrolytes, χ_{eff} follows a linear dependence on salt concentration as $\chi_{eff} = \chi_0 + mr$, where χ_0 is the interaction parameter of the neutral PS-*b*-POEGMA diblock copolymer and m is a system-dependent parameter.[13,15,17−20,31,38,40] An estimate of the phase state can be obtained by ignoring the presence of a small percentage of PAA. For the diblock copolymer electrolytes doped with LiTFSI, we employ $\chi_0^{\text{PS-}b\text{-POEGMA}} \sim 0.1$[31,38,40] (about half that of PS-*b*-PEO), $m \sim 0.2$[38,40] $r = 0.08$ (0.25), and $N = 55$ ($N_{\text{POEGMA}} + N_{\text{PS}}$), resulting in $\chi_{eff}N$ of 6.4 (8.3). The latter indicates a disordered phase state ($\chi_{eff}N < 20$ for neutral A−B diblock copolymer with $f_A \sim 0.8$). Hence, the effect of AA randomly distributed in the ion-containing phase is to increase the incompatibility between the nonionic and ionic blocks. This notion is based on the distinctly different interaction parameter, as $\chi_{\text{PS-PAA}}$ (=0.8122 + 21.55/T with $\chi_{\text{PS-PAA}} = 0.883$ at 303 K)[49] being much higher than $\chi_{\text{PS-POEGMA}}$ (~ 0.1 at 303 K).[31,38,40] Evidently, increasing the content of AA and further employing higher molar masses can increase the tendency for nanophase separation. Alternatively, in the case of much higher molar masses and copolymers with a higher AA content (both increase the tendency for phase separation), the Porod law limit (two-phase system with sharp boundaries) could be reached. Despite the low molar masses (Table 1), the presence of weakly ordered PS spheres in a matrix composed of the ion-containing phase allows for efficient ion transport (continuous 3D transport of Li ions) (see below).

III.IV. Ionic Conductivity and Mechanical Stability. For quantifying the impact of morphology, as well as the presence of AA on ion transport and the mechanical properties, dielectric spectroscopy and rheological measurements were carried out, respectively. Here, the dc-conductivity values were extracted from the plateau of $\sigma'(\omega)$ (Figure 6) (alternatively the Nyquist plot (Figure S10) can be employed). Specifically, the ionic conductivity for the electrolytes doped with LiTFSI increases by about 2 orders of magnitude.

The normalized ionic conductivity of the PS-*b*-P(AA-*co*-OEGA) electrolytes (by the volume fraction of the conductive
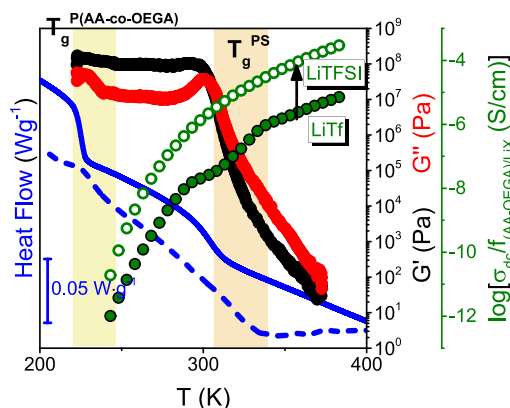

Figure 7. Composite diagram of the thermomechanical state in relation to the dc-conductivity. Temperature dependence of heat flow (rate = 10 K·min^{-1}) (blue line), normalized ionic conductivity by the volume fraction of the conductive phase (green symbols) and storage (black symbols), and loss (red symbols) moduli (rate = 5 K·min^{-1}, $\omega = 10$ rad·s^{-1}) for the PS-*b*-P(AA-*co*-OEGA) block-random copolymer electrolyte doped with LiTf (filled green symbols and solid lines) and LiTFSI (open green symbols and dashed lines) at a fixed salt concentration ($r = 0.08$).

phase) can be discussed with respect to Figures 7 and 8. The volume fraction of the "charged" block was calculated as[65]

$$f_{\text{(OEGA−AA)/LiX}} = \frac{v_{\text{OEGA−AA}} + rv_{\text{LiX}}}{v_{\text{OEGA−AA}} + rv_{\text{LiX}} + \left(\frac{M_{\text{PS}}M_{\text{OEGA−AA}}}{M_{\text{S}}M_{\text{POEGA−AA}}}\right)v_{\text{S}}}$$

(6)

Here, $v_i = M_i/\rho_i N_A$ is the volume of each phase, M_i is the molar mass of the repeat unit ($M_{\text{OEGA}} = 467.53$ g·mol^{-1}, $M_{\text{AA}} = 73.07$ g·mol^{-1}, $M_{\text{Styrene}} = 104.05$ g·mol^{-1}, $M_{\text{LiTf}} = 156.01$ g·mol^{-1}, $M_{\text{LiTFSI}} = 287.09$ g·mol^{-1}), and ρ_i is the density of each component ($\rho_{\text{OEGA}} = 1.10$ g·cm^{-3}, $\rho_{\text{AA}} = 1.4$ g·cm^{-3}, $\rho_{\text{Styrene}} = 1.04$ g·cm^{-3},
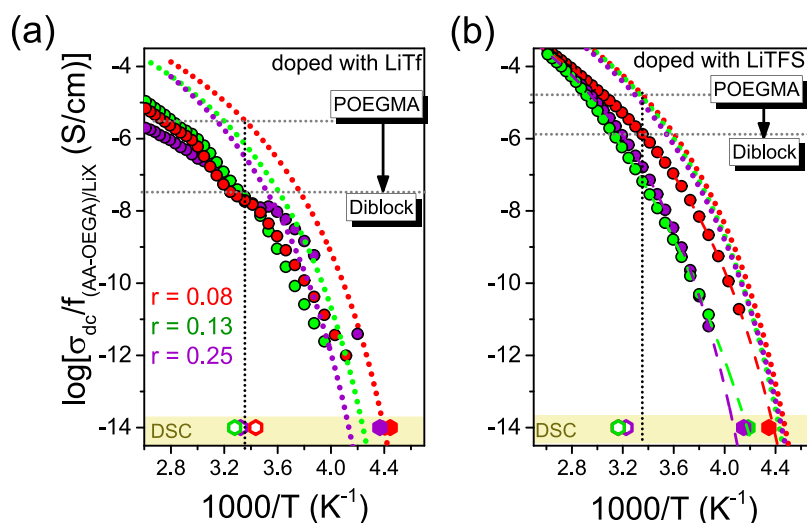
Figure 8. Normalized ionic conductivity by the volume fraction of the conductive phase P(AA-*co*-OEGA)/LiX plotted as a function of inverse temperature for the PS-*b*-P(AA-*co*-OEGA) block-random copolymer electrolytes doped with (a) LiTf and (b) LiTFSI at different salt concentrations; *r* = 0.08 (red symbols), *r* = 0.13 (green symbols), and *r* = 0.25 (purple symbols), obtained on heating. Dotted lines represent the ionic conductivities of the respective POEGMA homopolymer electrolytes. Dashed lines are fits to eq 2 for the block copolymer electrolytes doped with LiTFSI. Low and high calorimetric T_gs are shown at σ_{dc} of $\sim 10^{-14}$ S·cm^{-1} by filled and empty hexagons, respectively.

Table 2. Vogel−Fulcher−Tammann (VFT) Parameters of the dc-Conductivity and the Dielectric T_g for PS-*b*-P(AA-*co*-OEGA)/LiTFSI

$r = $ [Li$^+$]/[EO]	$-\log[\sigma_0$ (S·cm^{-1})]	B (K)	T_0 (K)	T_g (K)^a
0.08	0.48 ± 0.05	1450 ± 20	181.6 ± 0.8	228.2 ± 0.8
0.13	−2.4 ± 0.2	3100 ± 100	157 ± 3	239 ± 3
0.25	−0.25 ± 0.01	1673 ± 2	194.5 ± 0.1	245.5 ± 0.1

^{a}Dielectric T_g extracted at $\sigma_{dc} = 10^{-14}$ S·cm^{-1}.

ρ_{LiTf} = 2.136 g·cm^{-3}, ρ_{LiTFSI} = 2.392 g·cm^{-3}).[64−67] The volume fraction of the salt-containing phase amounts to ∼0.82.

Figure 7 compares the thermomechanical characteristics in relation to the ion conduction properties for the block-random copolymer electrolytes doped with LiTf or LiTFSI. In electrolytes doped with LiTf, the $\sigma_{dc}(T)$ is sensitive to the T_g^{PS} (non-VFT dependence in Figure 8a), suggesting that the transport of Li ions takes place also within the PS/P(AA-*co*-OEGA) interphase, as anticipated by SAXS (Figure 5). As a result, the maximum ionic conductivity, at an ambient temperature, is only ∼5 × 10^{-8} S·cm^{-1}. Parenthetically, Epps et al. report an ionic conductivity of 6 × 10^{-7} S·cm^{-1} (at $T = 293$ K = T_g + 63 K) for a PS-*b*-POEGMA diblock copolymer electrolyte doped with LiTf ($r \sim 0.06$).[48] Anion size has a strong effect on the morphology (Figure 5). Employing the weakly coordinated [TFSI$^-$], the $\sigma_{dc}(T)$ follows a VFT temperature dependence (Table 2), reflecting the transport of Li ions solely within the P(AA-*co*-OEGA) nanophase.

Figure 8 depicts the $\sigma_{dc}(T)$ for the diblock copolymer electrolytes doped with LiTf or LiTFSI with different Li salt concentrations. The DSC data, depicting the two T_gs, are also included (low and high T_gs are shown, respectively, by filled and empty symbols). The σ_{dc} at T_g can be estimated through the Nernst−Einstein equation as $\sigma_{dc} = \frac{ne^2d^2}{6\kappa_B T \tau}$, where n [= $\rho N_A/M_w$, where M_w is the molar mass of the ionic block including the conducting ions and ρ (∼1.6 g·cm^{-3})[64] is the density] is the number density of the mobile anions, d (= $R^+ + R^-$, where R^+ = R_{Li} = 0.076 nm, R^- = $R_{[TFSI]}$ ([Tf]) = 0.37 (0.28) nm)[53,68] is the distance between the [Li$^+$] and the [TFSI$^-$] or [Tf$^-$], assuming

contact pairs, τ is the characteristic relaxation time at T_g, and k_B is the Boltzmann constant. By employing τ = 100 s, the σ_{dc} at T_g amounts to ∼10^{-14} S·cm^{-1}.

The effect of AA incorporation along the POEGA backbone on ion conduction can be discussed with respect to the conductivity results of Figure 8b. At a fixed temperature, the dc-conductivity of PS-*b*-P(AA-*co*-OEGA)/LiTFSI decreases with increasing salt concentration, despite the absence of ion complexation with the EO side groups (Figures 2 and 8b). This reflects solely the anion/cation complexation with the carbonyl group (C=O) in PAA.[59,60] The latter restricts the backbone dynamics and increases the dielectric T_g (by about 18 K), as also evidenced by the DSC results (Figure 4). Apart from ion complexation, the increased intermolecular interactions via the H-bonding between AA and OEGA[69,70] significantly affect the backbone rigidity (Figures 7 and S11). Evidently, these factors have a small impact (by about 1 decade) on ion conduction due to the small percentage of AA and its random incorporation along the backbone. The main source of ion mobility is through the segmental mobility of EO side groups. As a result, the PS-*b*-P(AA-*co*-OEGA)/LiTFSI, with r = 0.08, exhibits relatively high ionic conductivities (∼ 10^{-6} S·cm^{-1}) at an ambient temperature.

The comparison of Li-ion conductivities, at a fixed Li salt concentration ($r \sim 0.08$) and at approximately the same temperature ($T \sim 293$ K), for different polymer electrolytes comprising linear and densely grafted architectures is made in Figure 9. Conductivities in the PS-*b*-P(AA-*co*-OEGA) copolymer when doped with LiTFSI are similar to reported systems but are more robust mechanically.
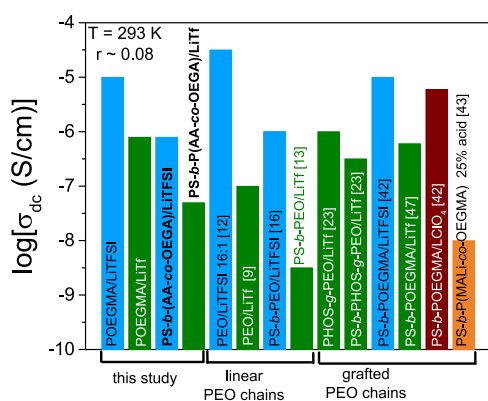
Figure 9. Comparison of Li-ion conductivities at a fixed Li salt concentration ($r \sim 0.08$) and at 293 K for different polymer electrolytes comprising linear and densely grafted architectures.

The rheological characteristics of the PS-b-P(AA-co-OEGA)/LiTf electrolyte, under isochronal conditions ($\omega = 10$ rad/s), nicely reflect the observed two calorimetric T_g''s. Precise information on the viscoelastic properties can be obtained by studying the frequency dependence of the storage and loss moduli at some selected temperatures above and below the T_g^{PS}. Such measurements require low strain amplitudes, corresponding to the linear viscoelastic regime (Figure S11). The frequency response of PS-b-P(AA-co-OEGA)/LiTf with $r = 0.08$ is purely elastic ($G' \gg G''$ and $G' \sim \omega^0$, $G'' \sim \omega^0$) at $T = 273$ and 293 K ($T < T_g^{PS}$). Parenthetically, at 273 K, the respective POEGMA electrolyte is liquid ($G' \sim \omega^2$ and $G'' \sim \omega^1$). At 323 K, a strong dependence on frequency is evidenced, reflecting the T_g^{PS}, i.e., the backbone stiffness of the ion-containing phase as well as the weakly ordered nanodomain morphology. At 353 K ($T > T_g^{PS}$), a typical terminal relaxation is observed ($G' \sim \omega^2$ and $G'' \sim \omega^1$), reflecting the low molar mass of the copolymer (Table 1). Importantly, at $T < T_g^{PS}$, the random diblock copolymer electrolyte doped with LiTf exhibits the preferred mechanical properties ($G' \sim 0.1$ GPa) for application as SPE, reflecting the presence of PS glassy domains combined with the mechanically robust P(AA-co-OEGA) phase. Noticeably, the storage moduli significantly increase (by about 4 orders of magnitude) as compared to the POEGMA homopolymer or PS-b-POEGMA diblock copolymer electrolytes with similar salt concentration (Figure S11b).[42] Overall, the incorporation of PAA provides a trade-off between the increased mechanical stability and cation/anion complexation with the PAA carbonyl group. The high mechanical stability suggests that they can be employed as films in batteries without the need for a separator.

Lastly, the thermomechanical, structural, and ion conduction properties of the PS-b-P(AA-co-OEGA) electrolytes are compared with those found in PS-b-P(AA-co-OEGA)-b-PS triblock copolymer electrolytes (bearing the same Li content). SAXS measurements revealed a weaker degree of segregation (mixing) between the PS and P(AA-co-OEGA) phases, as compared to the diblock case (Figure S12). As a result, at an ambient temperature, the dc-conductivity is reduced by 4 (one) orders of magnitude, as compared to the respective diblock copolymer PS-b-P(AA-co-OEGA) electrolytes doped with LiTFSI (LiTf) (Figures S13 and S14a). At the same time, the mechanical stability is maintained due to the presence of PS glassy domains and the increased stiffness of the P(AA-co-OEGA) backbone (Figure S14).

An important finding of the present investigation is that the POEGA block can be engineered to simultaneously support ion conduction (via the mobile EO/Li side groups) while maintaining mechanical stability. The final block-random grafted copolymer electrolytes with the incorporation of a small percentage of acid to the ion-containing block (as in P(AA-co-OEGA)) and the weakly coordinated anion, [TFSI⁻], can simultaneously provide mechanical stability ($G' \sim 10^8$ Pa) and relatively high ionic conductivity (up to $\sim 10^{-6}$ S·cm⁻¹) at an ambient temperature. Achieving similar conduction properties for the triblock copolymer electrolytes requires much higher molar masses.

IV. CONCLUSIONS

The successful synthesis of a series of block-random grafted copolymer electrolytes composed of the PS mechanical block and the ion-containing P(AA-co-OEGA) block facilitated a study of the effect of (i) acrylic acid incorporation into the ion-containing phase as well as of (ii) the anion type ([Tf⁻], [TFSI⁻]) on the thermomechanical, structural, and ion conduction properties. Importantly, the ion-containing P(AA-co-OEGA) block can independently provide ion conduction (via the mobile EO/Li side groups) and tunable mechanical properties (via the backbone stiffness). Moreover, despite the employed low molar masses, the existence of weakly ordered PS spheres in a matrix composed of the ion-containing phase facilitates the continuous 3D transport of Li ions. Between the two ions, the larger and weakly coordinated [TFSI⁻] is preferable for Li-ion conduction due to the suppression of ion complexation with the EO side groups. Summing up, the grafted copolymer electrolytes composed of an acid-containing charged block, doped with a weakly coordinated anion ([TFSI⁻]), simultaneously support mechanical stability ($G' \sim 10^8$ Pa) and relatively high dc-conductivity ($\sim 10^{-6}$ S·cm⁻¹) at an ambient temperature. For further triggering the nanophase separation and concomitantly increasing the ionic conductivity, future efforts would emphasize on the (i) acrylic acid content and (ii) higher molar masses. Overall, this work provides promising alternative ways for designing SPEs, which combine mechanical stability with relatively high ion conductivity, both of which are important to future battery technologies avoiding the need for a separator material.

◼ ASSOCIATED CONTENT

ⓈI Supporting Information

The Supporting Information is available free of charge at https://pubs.acs.org/doi/10.1021/acsapm.2c00987.

> Additional DSC, TM-DSC, XRD, SAXS, ionic conductivity, and rheological data for POEGMA, PS-b-P(AA-co-OEGA), and PS-b-P(AA-co-OEGA)-b-PS electrolytes doped with LiTf or LiTFSI (PDF)

◼ AUTHOR INFORMATION

Corresponding Authors

Stergios Pispas − *Theoretical and Physical Chemistry Institute, National Hellenic Research Foundation, 116 35 Athens, Greece;* ⓞ orcid.org/0000-0002-5347-7430; Email: pispas@eie.gr

George A. Floudas − *Department of Physics, University of Ioannina, 451 10 Ioannina, Greece; Institute of Materials Science and Computing, University Research Center of Ioannina (URCI), 451 10 Ioannina, Greece; Max Planck*

Institute for Polymer Research, 55128 Mainz, Germany;
 orcid.org/0000-0003-4629-3817; Email: gfloudas@
uoi.gr

Authors

> **Achilleas Pipertzis** − *Department of Physics, University of Ioannina, 451 10 Ioannina, Greece*
>
> **Martha Kafetzi** − *Theoretical and Physical Chemistry Institute, National Hellenic Research Foundation, 116 35 Athens, Greece*
>
> **Despoina Giaouzi** − *Theoretical and Physical Chemistry Institute, National Hellenic Research Foundation, 116 35 Athens, Greece*

Complete contact information is available at:
https://pubs.acs.org/10.1021/acsapm.2c00987

Notes

The authors declare no competing financial interest.

■ REFERENCES

(1) Goodenough, J. B. Electrochemical Energy Storage in a Sustainable Modern Society. *Energy Environ. Sci.* **2014**, *7*, 14−18.

(2) Goodenough, J. B.; Park, K-S. Li-ion battery: A perspective. *J. Am. Chem. Soc.* **2013**, *135*, 1167−1176.

(3) Goodenough, J. B.; Kim, Y. Challenges for Rechargeable Li Batteries. *Chem. Mater.* **2010**, *22*, 587−603.

(4) Tarascon, J. M.; Armand, M. Issues and Challenges Facing Rechargeable Lithium Batteries. *Nature* **2001**, *414*, 359−367.

(5) Zhou, D.; Shanmukaraj, D.; Tkacheva, A.; Armand, M.; Wang, G. Polymer Electrolytes for Lithium-Based Batteries: Advances and Prospects. *Chem* **2019**, *5*, 2326−2352.

(6) Lascaud, S.; Perrier, M.; Vallee, A.; Besner, S.; Prud'homme, J.; Armand, M. Phase Diagrams and Conductivity Behavior of Poly-(ethylene oxide)-Molten Salt Rubbery Electrolytes. *Macromolecules* **1994**, *27*, 7469−7477.

(7) Hayamizu, K.; Akiba, E.; Bando, T.; Aihara, Y. ^1H, ^7Li, and ^{19}F Nuclear Magnetic Resonance and Ionic Conductivity Studies for Liquid Electrolytes Composed of Glymes and Polyetheneglycol Dimethyl Ethers of $CH_3O(CH_2CH_2O)_nCH_3$ (x =3-50) Doped with LiN-(SO_2CF_3)2. *J. Chem. Phys.* **2002**, *117*, 5929−5939.

(8) Teran, A. A.; Tang, M. H.; Mullin, S. A.; Balsara, N. P. Effect of Molecular Weight on Conductivity of Polymer Electrolytes. *Solid State Ionics* **2011**, *203*, 18−21.

(9) Zardalidis, G.; Ioannou, E.; Pispas, S.; Floudas, G. Relating Structure, Viscoelasticity, and Local Mobility to Conductivity in PEO/LiTf Electrolytes. *Macromolecules* **2013**, *46*, 2705−2714.

(10) Timachova, K.; Watanabe, H.; Balsara, N. P. Effect of Molecular Weight and Salt Concentration on Ion Transport and the Transference Number in Polymer Electrolytes. *Macromolecules* **2015**, *48*, 7882−7888.

(11) Xue, Z.; He, D.; Xie, X. Poly(ethylene oxide)-Based Electrolytes for Lithium-ion Batteries. *J. Mater. Chem. A* **2015**, *3*, 19218−19253.

(12) Tu, C.-H.; Veith, L.; Butt, H.-J.; Floudas, G. Ionic Conductivity of a Solid Polymer Electrolyte Confined in Nanopores. *Macromolecules* **2022**, *55*, 1332−1341.

(13) Zardalidis, G.; Gatsouli, K.; Pispas, S.; Mezger, M.; Floudas, G. Ionic Conductivity, Self-Assembly, and Viscoelasticity in Poly(styrene-*b*-ethylene oxide) Electrolytes Doped with LiTf. *Macromolecules* **2015**, *48*, 7164−7171.

(14) Panday, A.; Mullin, S.; Gomez, E. D.; Wanakule, N.; Chen, V. L.; Hexemer, A.; Pople, J.; Balsara, N. P. Effect of Molecular Weight and Salt Concentration on Conductivity of Block Copolymer Electrolytes. *Macromolecules* **2009**, *42*, 4632−4637.

(15) Wanakule, N. S.; Virgili, J. M.; Teran, A. A.; Wang, Z.-G.; Balsara, N. P. Thermodynamic Properties of Block Copolymer Electrolytes Containing Imidazolium and Lithium Salts. *Macromolecules* **2010**, *43*, 8282−8289.

(16) Yuan, R.; Teran, A. A.; Gurevitch, I.; Mullin, S. A.; Wanakule, N. S.; Balsara, N. P. Ionic Conductivity of Low Molecular Weight Block Copolymer Electrolytes. *Macromolecules* **2013**, *46*, 914−921.

(17) Young, W.-S.; Kuan, W.-F.; Epps, T. H., III. Block Copolymer Electrolytes for Rechargeable Lithium Batteries. *J. Polym. Sci., Part B: Polym. Phys.* **2014**, *52*, 1−16.

(18) Teran, A. A.; Balsara, N. P. Thermodynamics of Block Copolymers With and Without Salt. *J. Phys. Chem. B* **2014**, *118*, 4−17.

(19) Loo, W. S.; Galluzzo, M. D.; Li, X.; Maslyn, J. A.; Oh, H. J.; Mongcopa, K. I.; Zhu, C.; Wang, A. A.; Wang, X.; Garetz, B. A.; Balsara, N. P. Phase Behavior of Mixtures of Block Copolymers and a Lithium Salt. *J. Phys. Chem. B* **2018**, *122*, 8065−8074.

(20) Loo, W. S.; Balsara, N. P. Organizing Thermodynamic Data Obtained from Multicomponent PolymerElectrolytes: Salt-Containing Polymer Blends and Block Copolymers. *J. Polym. Sci., Part B: Polym. Phys.* **2019**, *57*, 1177−1187.

(21) Dreier, P.; Pipertzis, A.; Spyridakou, M.; Mathes, R.; Floudas, G.; Frey, H. Introduction of Trifluoromethanesulfonamide Groups in Poly(ethylene oxide): Ionic Conductivity of Single-Ion-Conducting Block Copolymer Electrolytes. *Macromolecules* **2022**, *55*, 1342−1353.

(22) Hadjichristidis, N.; Pispas, S.; Floudas, G. *Block Copolymers: Synthetic Strategies, Physical Properties and Applications*; Wiley Interscience: New York, 2002.

(23) Zardalidis, G.; Pipertzis, A.; Mountrichas, G.; Pispas, S.; Mezger, M.; Floudas, G. Effect of Polymer Architecture on the Ionic Conductivity. Densely Grafted Poly(ethylene oxide) Brushes Doped with LiTf. *Macromolecules* **2016**, *49*, 2679−2687.

(24) Devaux, D.; Glé, D.; Phan, T. N. T.; Gigmes, D.; Giroud, E.; Deschamps, M.; Denoyel, R.; Bouchet, R. Optimization of Block Copolymer Electrolytes for Lithium Metal Batteries. *Chem. Mater.* **2015**, *27*, 4682−4692.

(25) Bates, C. M.; Chang, A. B.; Momčilović, N.; Jones, S. C.; Grubbs, R. H. ABA Triblock Brush Polymers: Synthesis, Self-Assembly, Conductivity, and Rheological Properties. *Macromolecules* **2015**, *48*, 4967−4973.

(26) Saladaga, I. A.; Janthasit, S.; de Luna, M. D. G.; Grisdanurak, N.; Tantrawong, S.; Paoprasert, P. Poly(oligoethylene Glycol Methacrylate): A Promising Electrolyte Polymer. *Chiang Mai J. Sci.* **2015**, *42*, 868−876.

(27) Bartels, J.; Wang, J-H. H.; Chen, Q.; Runt, J.; Colby, R. H. Segmental Dynamics of Ethylene Oxide-Containing Polymers with Diverse Backbone Chemistries. *Macromolecules* **2016**, *49*, 1903−1910.

(28) Wang, X.; Song, Z.; Wu, H.; Nie, J.; Feng, W.; Yu, H.; Huang, X.; Armand, M.; Zhou, Z.; Zhang, H. Unprecedented Impact of Main Chain on Comb Polymer Electrolytes Performances. *ChemElectroChem* **2022**, *9*, No. e20210159.

(29) Pipertzis, A.; Papamokos, G.; Sachnik, O.; Allard, S.; Scherf, U.; Floudas, G. Ionic Conductivity in Polyfluorene-Based Diblock Copolymers Comprising Nanodomains of a Polymerized Ionic Liquid and a Solid Polymer Electrolyte Doped with LiTFSI. *Macromolecules* **2021**, *54*, 4257−4268.

(30) Kuan, W-F.; Remy, R.; Mackay, M. E.; Epps, T. H. Controlled Ionic Conductivity via Tapered Block Polymer Electrolytes. *RSC Adv.* **2015**, *5*, 12597.

(31) Kuan, W. F.; Reed, E. H.; Nguyen, N. A.; Mackay, M. E.; Epps, T. H. Using Tapered Interfaces to Manipulate Nanoscale Morphologies in Ion-doped Block Polymers. *MRS Commun.* **2015**, *5*, 251−256.

(32) Ketkar, P. M.; Shen, K-H.; Fan, M.; Hall, L. M.; Epps, T. H. Quantifying the Effects of Monomer Segment Distributions on Ion Transport in Tapered Block Polymer Electrolytes. *Macromolecules* **2021**, *54*, 7590−7602.

(33) Galanos, E.; Wahlen, C.; Butt, H.-J.; Frey, H.; Floudas, G. Phase Diagram of Tapered Copolymers Based on Isoprene and Styrene. *Macromol. Chem. Phys.* **2022**, *223*, No. 2200033.

(34) Hoang Thi, T. T.; Pilkington, E. H.; Nguyen, D. H.; Lee, J. S.; Park, K. D.; Truong, N. P. The Importance of Poly(ethylene glycol) Alternatives for Overcoming PEG Immunogenicity in Drug Delivery and Bioconjugation. *Polymers* **2020**, *12*, 298.

(35) Kafetzi, M.; Pispas, S.; Bao, X.; Yao, P. Amphiphilic QP-(DMAEMA-*co*-LMA)-*b*-POEGMA Random-block Terpolymers as Nanocarriers for Insulin. *Biomedicines* **2020**, *8*, No. 392.

(36) Kafetzi, M.; Pispas, S. Effects of Hydrophobic Modifications on the Solution Self-Assembly of P(DMAEMA-*co*-QDMAEMA)-b-POEGMA Random Diblock Copolymers. *Polymers* **2021**, *13*, 338.

(37) Chroni, A.; Mavromoustakos, T.; Pispas, S. Nano-Assemblies from Amphiphilic PbBA-*b*-POEGA Copolymers as Drug Nanocarriers. *Polymer* **2021**, *13*, No. 1164.

(38) Gartner, T. E.; Morris, M. A.; Shelton, C. K.; Dura, J. A.; Epps, T. H. Quantifying Lithium Salt and Polymer Density Distributions in Nanostructured Ion-Conducting Block Polymers. *Macromolecules* **2018**, *51*, 1917−1926.

(39) Shim, J.; Bates, F. S.; Lodge, T. P. Superlattice by Charged Block Copolymer Self-Assembly. *Nat. Commun.* **2019**, *10*, No. 2108.

(40) Zhang, B.; Zheng, C.; Sims, M. B.; Bates, F. S.; Lodge, T. P. Influence of Charge Fraction on the Phase Behavior of Symmetric Single-Ion Conducting Diblock Copolymers. *ACS Macro Lett.* **2021**, *10*, 1035−1040.

(41) Ishizone, T.; Han, S.; Hagiwaka, M.; Yokoyama, H. Synthesis and Surface Characterization of Well-Defined Amphiphilic Block Copolymers Containing Poly(oligo ethylene glycol methacrylate) Segments. *Macromolecules* **2006**, *39*, 962−970.

(42) Rolland, J.; Brassinne, J.; Bourgeois, J.-P.; Poggi, E.; Vlad, A.; Gohy, J-F. Chemically Anchored Liquid-PEO Based Block Copolymer Electrolytes for Solid-state Lithium-ion Batteries. *J. Mater. Chem. A.* **2014**, *2*, 11839.

(43) Rolland, J.; Poggi, E.; Vlad, A.; Gohy, J.-F. Single-ion Diblock Copolymers for Solid-State Polymer Electrolytes. *Polymer* **2015**, *68*, 344−352.

(44) Bergman, M.; Bergfelt, A.; Sun, B.; Bowden, T.; Brandell, D.; Johanson, P. Graft Copolymer Electrolytes for High Temperature Li-battery Applications, Using Poly(methyl methacrylate) Grafted Poly(ethylene glycol)methyl Ether Methacrylate and Lithium bis (trifluoromethanesulfonimide). *Electrochem. Acta* **2015**, *175*, 96−103.

(45) Daigle, J.-C.; Vijh, A.; Hovington, P.; Gagnon, C.; Hamel-Paquet, J.; Verreault, S.; Turcotte, N.; Clement, D.; Guerfi, A.; Zaghib, K. Lithium Battery with Solid Polymer Electrolyte based on Comb-like Copolymers. *J. Power Sources* **2015**, *279*, 372−383.

(46) Bergfelt, A.; Rubatat, L.; Brandell, D.; Bowden, T. Poly(benzyl methacrylate)-Poly[(oligo ethylene glycol) Methyl Ether Methacrylate] Triblock-Copolymers as Solid Electrolyte for Lithium Batteries. *Solid State Ionics* **2018**, *321*, 55−61.

(47) Morris, M. A.; Sung, S. H.; Ketkar, P. M.; Dura, J. A.; Nieuwendaal, R. C.; Epps, T. H. Enhanced Conductivity via Homopolymer-Rich Pathways in Block Polymer-Blended Electrolytes. *Macromolecules* **2019**, *52*, 9682−9692.

(48) Yu, D. M.; Smith, D. M.; Kim, H.; Rzayev, J.; Russell, T. P. Two-step Chemical Transformation of Polystyrene-block-polysolketal acrylate) Copolymers for Increasing χ. *Macromolecules* **2019**, *52*, 6458−6466.

(49) Kremer, F.; Schönhals, A., *Broadband Dielectric Spectroscopy*; Springer 2002: Berlin, 2003, DOI: DOI: 10.1007/978-3-642-56120-7.

(50) Floudas, G. Dielectric Spectroscopy. In *Polymer Science: A Comprehensive Reference*; Matyjaszewski, K.; Möller, M., Eds.; Elsevier B. V.: Amsterdam, 2012; Vol. 2 32, pp 825−845.

(51) Dyre, J. C. The Random Free-Energy Barrier Model for ac Conduction in Disordered Solids. *J. Appl. Phys.* **1988**, *64*, 2456−2468.

(52) Schröder, T. B.; Dyre, J. C. Ac Hopping Conduction at Extreme Disorder Takes Place on the Percolating Cluster. *Phys. Rev. Lett.* **2008**, *101*, No. 025901.

(53) Pipertzis, A.; Papamokos, G.; Mühlinghaus, M.; Mezger, M.; Scherf, U.; Floudas, G. What Determines the Glass Temperature and dc-Conductivity in Imidazolium-Polymerized Ionic Liquids with a Polythiophene Backbone? *Macromolecules* **2020**, *53*, 3535−3550.

(54) Mauger, A.; Julien, C. M.; Paolella, A.; Armand, M.; Zaghib, K. A Comprehensive Review of Lithium Salts and Beyond for Rechargeable Batteries: Progress and Perspectives. *Mater. Sci. Eng., R* **2018**, *134*, 1−21.

(55) Shiau, H.-S.; Liu, W.; Colby, R. H.; Janik, M. J. Cluster Continuum Quantum Mechanical Models to Guide the Choice of Anions for Li⁺-Conducting Ionomers. *J. Chem. Phys.* **2013**, *139*, 204905.

(56) Tkachenko, V.; Kunemann, P.; Malval, J. P.; Petithory, T.; Pieuchot, L.; Vidal, L.; Chemtob, A. Kinetically Stable sub-50 nm Fluorescent Block Copolymer Nanoparticles via Photomediated RAFT Dispersion Polymerization for Cellular Imaging. *Nanoscale* **2022**, *14*, 534−545.

(57) Floudas, G.; Štepánek, P. Structure and Dynamics of Poly(*n*-decyl methacrylate) Below and Above the Glass Transition. *Macromolecules* **1998**, *31*, 6951−6957.

(58) Fox, T. G.; Flory, P. J. Second-Order Transition Temperatures and Related Properties of Polystyrene. I Influence of Molecular Weights. *J. Appl. Phys.* **1950**, *21*, 581.

(59) Kam, W.; Liew, C.-W.; Lim, J. Y.; Ramesh, S. Electrical, Structural, and Thermal Studies of Antimony Trioxide-doped Poly-(acrylic acid)-based Composite Polymer Electrolytes. *Ionics* **2014**, *20*, 665−674.

(60) Liew, C.-W.; Ng, H. M.; Numan, A.; Ramesh, S. Poly(Acrylic acid)−Based Hybrid Inorganic−Organic Electrolytes Membrane for Electrical Double Layer Capacitors Application. *Polymers* **2016**, *8*, 179.

(61) Kinning, D. J.; Thomas, E. L. Hard-Sphere Interactions between Spherical Domains in Diblock Copolymers. *Macromolecules* **1984**, *17*, 1712−1718.

(62) Bourlinos, A. B.; Giannelis, E. P.; Zhang, Q.; Archer, L. A.; Floudas, G.; Fytas, G. Surface-functionalized Nanoparticles with Liquid-like Behavior: The Role of the Constituent Components. *Eur. Phys. J. E.* **2006**, *20*, 109−117.

(63) Rubinstein, M.; Colby, R. H. *Polymer Physics*; Oxford University Press: Oxford, 2003.

(64) Van Krevelen, D. W.; Hoftyzer, P. J. Prediction of Polymer Densities. *J. Appl. Polym. Sci.* **1969**, *13*, 871−881.

(65) Sethi, G. K.; Jung, H. Y.; Loo, W. S.; Sawhney, S.; Park, M. J.; Balsara, N. P.; Villaluenga, I. Structure and Thermodynamics of Hybrid Organic−Inorganic Diblock Copolymers with Salt. *Macromolecules* **2019**, *52*, 3165−3175.

(66) (a) Ponchel, G.; Touchard, F.; Duchene, D.; Peppas, N. A. Bioadhesive Analysis of Controlled-Release Systems. I. Fracture and Interpenetration Analysis in Poly(acrylic acid)-Containing Systems. *J. Controlled Release* **1987**, *5*, 129−141;(b) *Chem. − Eur. J.* **2007**, *36*, 4536−4549.

(67) Mark, J. E. *Physical Properties of Polymers Handbook*; 2nd ed.; Springer−Verlag: New York, 1996.

(68) Masahiro, Y.; Hiroaki, H.; Haruna, T.; Naohide, M.; Massaki, M.; Francoise, D.; Jean-Pierre, T.; Nazzareno, R.; Seiichiro, I. A Variety of Spin-Crossover Behaviors Depending on the Counter Anion: Two-Dimensional Complexes Constructed by NH···Cl⁻ Hydrogen Bonds, [Fe^{II}H$_3$L^{Me}]Cl·X (X = PF$_6$⁻, AsF$_6$−, SbF$_6$⁻, CF$_3$SO$_3$⁻; H$_3$L^{Me} = Tris[2-{[(2-methylimidazol-4-yl)methylidene]amino}ethyl]amine). *Chem. − Eur. J.* **2006**, *12*, 4536−4549.

(69) Jo, G.; Ahn, H.; Park, M. J. Simple Route for Tuning the Morphology and Conductivity of Polymer Electrolytes: One end Functional Group is Enough. *ACS Macro Lett.* **2013**, *2*, 990−995.

(70) Wang, R.-Y.; Huang, J.; Guo, X.-S.; Cao, X.-H.; Zou, S.-F.; Tong, Z.-Z.; Xu, J.-T.; Du, B.-Y.; Fan, Z.-Q. Closed-Loop Phase Behavior of Block Copolymers in the Presence of Competitive Hydrogen-Bonding and Coulombic Interaction. *Macromolecules* **2018**, *51*, 4727−4734.